Dynamic evolution of discommensurations during the commensurate-incommensurate transition in barium sodium niobate

1990 J. Phys.: Condens. Matter 2 2603

(http://iopscience.iop.org/0953-8984/2/11/007)

J. Phys.: Condens. Matter **2** (1990) 2603–2623. Printed in the UK

Dynamic evolution of discommensurations during the commensurate–incommensurate transition in barium sodium niobate

Xiaoqing Pan†‡, H Gleiter† and Duan Feng‡

† Institute of New Materials, University of Saarland, D-6600 Saarbrucken, Federal Republic of Germany

‡ Institute of Solid State Physics, Nanjing University, Nanjing, People's Republic of China

Received 3 January 1989, in final form 10 August 1989

Abstract. The temperature evolution of discommensurations (DC) during the heating run through the commensurate–incommensurate (C-I) transition in barium sodium niobate is investigated by means of transmission electron microscopy. It is found that the interaction of DC is attractive over considerable distances, and that frozen-in DC become meandering and collide with each other in the process of reducing the DC density under the influence of thermal fluctuations at a temperature below the lock-in transition. A transient metastable state (or chaotic state) is observed with successive nucleation of DC in the early stages of transition, and later a wavy DC array is formed. DC loops with high density of DC are formed at a temperature above the C-I transition. A qualitative theoretical explanation of the observed characteristics on the evolution of DC is presented based on a Landau theory.

1. Introduction

The existence of a multi-soliton lattice in the low-temperature part of incommensurate (I) phases is now well established. Locally commensurate (C) regions are separated by discommensurations (DC) where the phase and amplitude of the modulation wave change abruptly [1, 2]. The commensurate–incommensurate (C-I) transition at temperature T_L is predicted to be continuous in the constant-amplitude approximation, but may become discontinuous if amplitude variations or additional degrees of freedom coupled to the order parameter are taken into account in the thermodynamic potential [3]. It is generally believed that transformation during the C-I transition proceeds through nucleation or annihilation of DC. In the vicinity of T_L the discreteness of the crystal lattice and the influence of extrinsic defects may become important and may induce an intermediate regime where the states are spatially chaotic. In the following work an experimental study of such processes in barium sodium niobate (BSN) and some qualitative theoretical interpretations of their underlying mechanism are presented.

Some of the main features of the system studied are briefly summarised. An intricate pattern of phase transitions has been observed in BSN, and is schematically displayed in table 1. A standard ferroelectric transition (P4/m*b*m–P4*b*m) occurs at about 580 °C [4]. Two transitions separated by about 50 °C are located near 250 and 300 °C and bound the I phase possessing an average orthorhombic point symmetry [5, 6]. This point symmetry

0953-8984/90/112603 + 21 $03.50

Table 1. The phases and related phase transitions in barium sodium niobate.

Ferroelectric phase					Paraelectric phase
Paraelastic phase	Ferroelastic phase			Paraelastic phase	
Tetragonal symmetry P4*b*m[6] (?)	Orthorhombic symmetry B*bm*2[5] $a_0 = 35.2$ Å $b_0 = 17.62$ Å $c_0 = 8$ Å C phase Frozen-in DC	$\delta = 1\%–10\%$ I phase Nucleation and growth of stripples		Tetragonal symmetry P4*b*m Polarisation along *c* axis N phase	Tetragonal symmetry P4/m*b*m $a_t = 12.4$ Å $b_t = 12.4$ Å $c_t = 4$ Å
Ferroelastic transition(?) T_1' (≃ −160 °C)	C–I transition T_L (≃250 °C)		I–N (ferroelastic) transition T_1 (≃300 °C)	Ferroelectric transition T_O (≃580 °C)	

persists down to −160 °C where another transformation restores tetragonal symmetry [7]. According to electron microscopic observations [8–10], the DC in incommensurate BSN are irregularly distributed in space with an average direction perpendicular to modulation [8–10]. The lenticularly shaped nuclei of DC are generated at a temperature slightly above T_L, and grow in size with increasing temperature [11]. Other phenomena related to the presence of the I phase but departing from the standard behaviour expected for incommensurate systems had been noticed [6, 12], such as a large thermal hysteresis of a specific type, slow time-relaxation processes and a 'memory effect'. These phenomena are currently assigned [12] to the occurrence of an interaction between the incommensurate modulation and mobile point defects. The occurrence of pinning on the DC pattern by stoichiometric defects and defects induced by electron-beam irradiation have recently been studied by transmission electron microscopy [10, 13–15]. Obviously, it is an interesting problem to study how the pinned DC affect the C–I transition and the evolution of DC in temperature and time if the system is thermally cycled through the C–I transition. The present investigations contribute to an understanding of such aspects. We have examined the patterns of DC in BSN between ambient temperature and the normal–incommensurate (N–I) transition (~300 °C) by transmission electron microscopy (TEM) and attempted a theoretical interpretation of the underlying mechanisms.

The plan of the paper is as follows. In section 2 the experimental procedure is briefly described and in section 3 the experimental results obtained by transmission electron microscopy are presented. In section 4 the results obtained in section 3 are considered from the perspective of a qualitative theory of the C–I phase transition. Conclusions and an outlook are presented in section 5.

2. Experimental methods

The single crystals of BSN used had the same origin as those studied in the previous experiments [8, 11]. Disc-shaped samples with (0 0 1) orientation (3 mm diameter and 0.10–0.15 mm thick) were mechanically polished to a thickness of about 30 μm, and were thinned further to about 100 nm by Ar^+ ion bombarding at an operating voltage of 6 kV at an incident angle of about 12°. *In situ* observations were achieved with a JEOL JEM-200CX electron microscope at an accelerating voltage of 200 kV, using a side-entry hot stage.

3. Results

Dark-field images of DC in BSN obtained at different temperatures by selecting incommensurate–satellite reflections during several thermal cycles starting from ambient temperature have been observed (figure 1), displaying a similar type of pattern as described in several recent TEM observations of BSN [8–10, 14]. The patterns have the form of wavy lines, generally directed along either [1 1 0] or [1 $\bar{1}$ 0] corresponding to different ferroelastic domains (referred to the axes of the normal tetragonal phase), although the regularity observed in each domain is poor. In the following we will refer to such structures as wavy DC patterns. It is easily deduced from figure 1(*a*) that frozen-in DC tend to run close to each other, producing a filamentary structure, so that there is no regular DC lattice to be observed. A similar characteristic can also be observed in the configurations of newly generated DC at a temperature slightly above T_L, as shown in

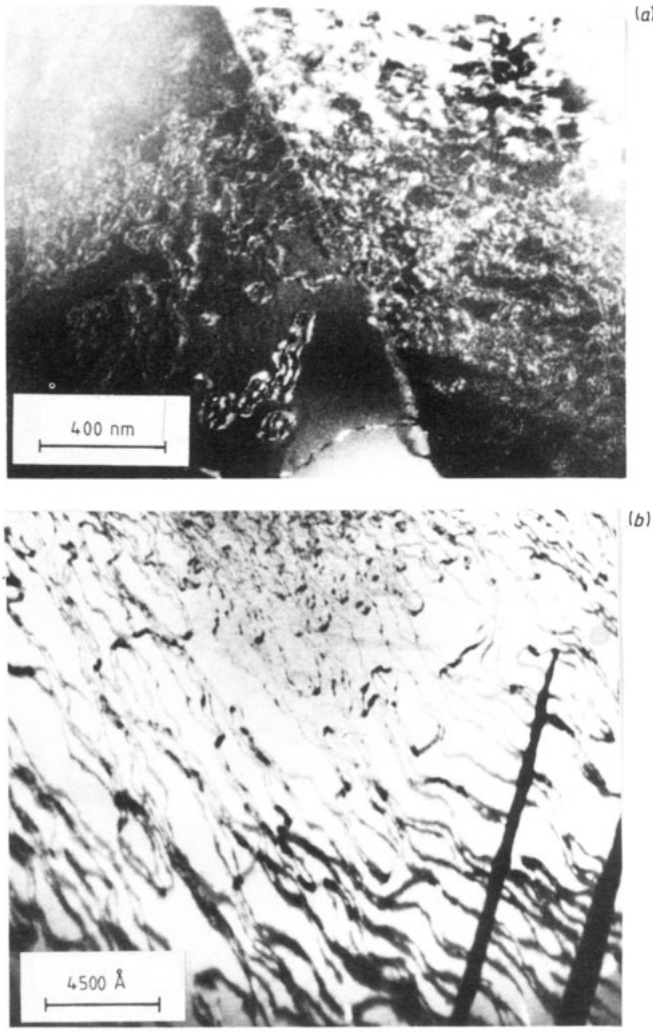

Figure 1. Dark-field micrographs obtained by selecting incommensurate satellite reflections taken at different temperatures. (*a*) Ambient temperature. (*b*) At about 230 °C. It clearly shows that both frozen-in DC (*a*) and newly generated DC (*b*) tend to run close to each other, implying that there is an attractive interaction between neighbouring DC in BSN.

figure 1(*b*) (figure 2 in [11]). As was pointed out in [11], the lenticularly shaped nuclei of DC can easily extend in the direction perpendicular to the modulation wavevector, but hardly parallel to this direction. Thus, it is plausible to assume that the DC in BSN have an attractive interaction over a considerable distance, which may result in the C–I transition being discontinuous [3]. (The attractive or repulsive interaction of DC has two origins and will be discussed in section 4.) This is consistent with the experimental observations on the C–I transition by means of different methods [8, 12], and with the phenomenological description of the C–I transition [3], where the coupling of the order parameter to the strain tensor in the thermodynamic potential was considered.

The temperature evolution of pinned (or frozen-in) DC from ambient temperature to about 230 °C is shown in figures 2(*a*)–(*c*). As was reported previously [8, 11], the configurations of pinned DC (figure 2(*a*)) undergo no apparent change during the heating run up to about 200 °C. Two remarkable features of the frozen-in DC structure are worth mentioning. First, there are four-fold sources and sinks, depending on sign conventions, where DC emanate or vanish. These will be called vortices in the following. The set of

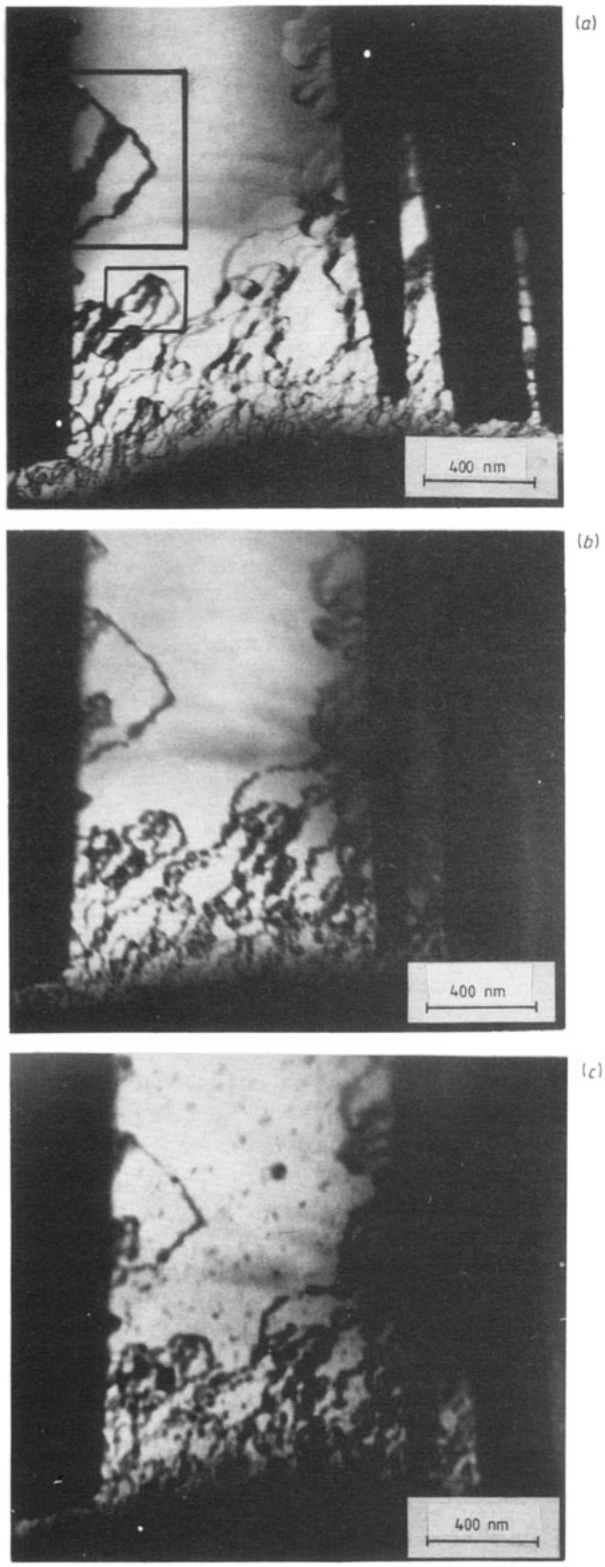

Figure 2. Dark-field micrographs taken at different temperatures in the same area of a sample show the evolution of frozen-in DC under the influence of thermal fluctuations. (*a*) Ambient temperature. (*b*) At 210 °C. Note that DC become meandering (or roughening) with increasing temperature and undergo collisions with their neighbours, which leads to their annihilation or fusion. (*c*) At 230 °C. Note the nucleation of DC as black droplets in (*c*).

vortices is connected by DC in an irregular fashion and thus suspends a multiconnected network similar to that in vulcanised rubber. Secondly, DC connecting two vortices are not straight but curved and some are irregularly shaped. From the first feature it follows that the network of DC cannot easily annihilate due to topological obstructions, whereas the second feature implies that DC are locally pinned and not only suspended by the vortices. Owing to the finite size of the specimens studied the DC will in reality be membrane-shaped and are suspended by vortex segments. Accordingly in the following we will refer to the DC also as domain walls.

With the temperature rising further and approaching 230 °C, a strong influence of thermal fluctuations on pinned DC patterns is observed. Figure 2(*b*) was taken at about 210 °C in the same area as in figure 2(*a*), and figure 2(*c*) at a temperature slightly above 230 °C. Figure 3(*a*) shows schematically the phase change of the DC in the upper left-hand side of figure 2(*a*). Accordingly, the sign of DC is conveniently (for practical purposes) defined in such a way that it is positive for one having a positive phase jump passing through it along the modulation direction, and negative for that (anti-soliton) having a negative phase jump. More accurately we define the charge of a vortex as $\sigma \equiv \Delta\varphi/2\pi$, where $\Delta\varphi$ is the phase change experienced by an observer upon sur-

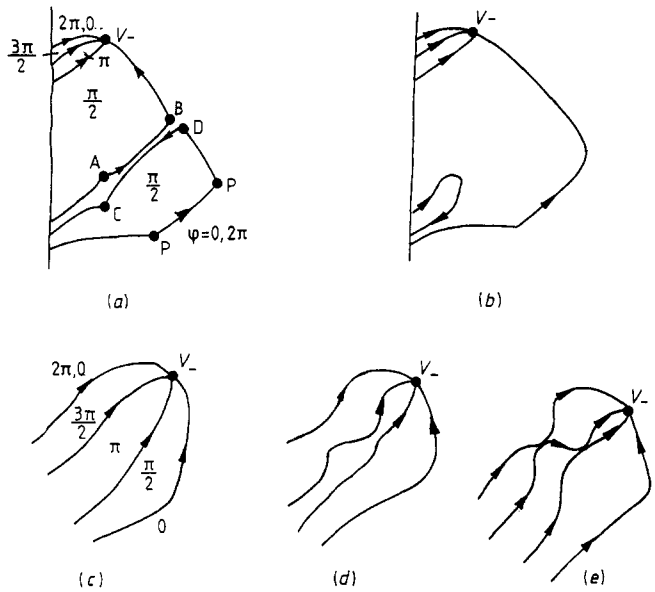

Figure 3. Schematic plot of processes of DC collision occurring in the region marked by a box in the upper left-hand side of figure 2(*a*). Here (*a*) and (*b*) illustrate that two segments (AB and CD) of DC with opposite orientations annihilate after their collision. (*c*) This shows a vortex and the four DC emanating from it. The numbers refer to the phase of the order parameter in the respective domain. The arrows indicate the orientation of DC as explained in the text. (*d*) and (*e*) DC with the same sign of phase change or say the same orientation can also contact each other along finite segments under the influence of thermal fluctuations.

Figure 4 (opposite). Dark-field micrographs, taken at different temperatures in the same area of a sample, show the dynamic evolution of newly created DC in BSN. (*a*) At ambient temperature. Note the configuration of frozen-in DC which are randomly distributed due to strong pinning by defects. (*b*) At about 230 °C. Note the appearance of DC nuclei as dark objects (or white, depending on the condition of imaging). (*c*) Taken at the same temperature as (*b*), but several minutes later. (*d*) and (*e*) Taken at about 250 °C several minutes apart. Note that (*e*) shows clearly the wavy DC array. (*f*) At about 260 °C. The time evolution of DC takes place in the form of growth of DC nuclei towards their thermal equilibrium configuration, and the temperature evolution of DC occurs over an increase of DC density on increasing the temperature. The nucleation and distribution of DC in the sample is inhomogeneous, and is accompanied by a large thermal hysteresis of DC density, which results in the existence of metastable states (chaotic state).

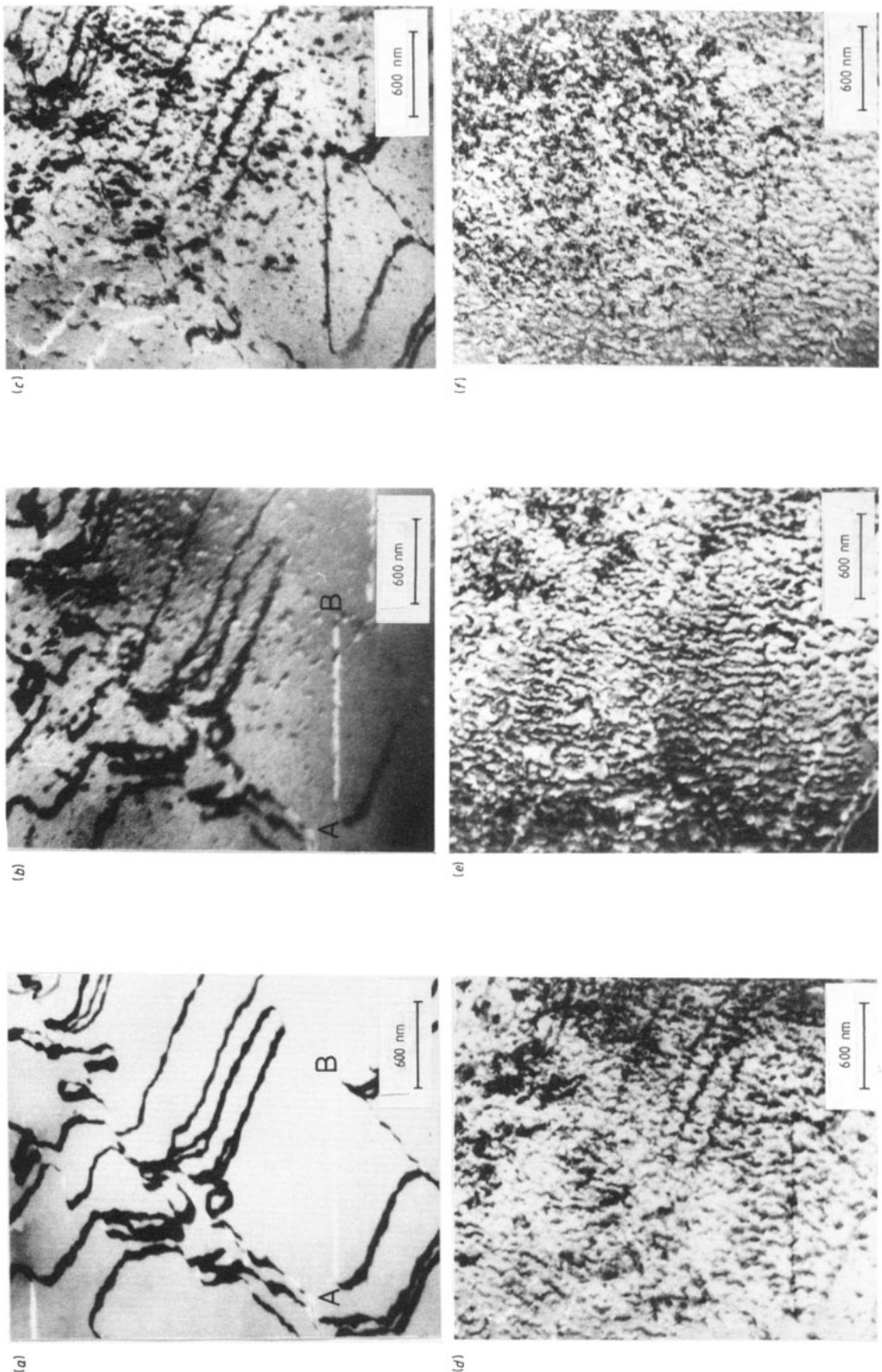
600 nm
A
B
(a)
(b)
(c)
(d)
(e)
(f)

rounding the vortex anticlockwise. Vortices (+) and antivortices (−) are produced or annihilated pairwise. DC emanate from vortices (+) and flow into antivortices (−). This provides DC with a natural orientation indicated by an arrow in figure 3. DC with opposite orientation can annihilate but DC with the same orientation cannot.

It is noticed from figures 2(*a*) and (*b*) that DC become wandering (or roughening) under the influence of thermal fluctuations and collide with their neighbours. The collisions lead to two different final states depending on whether the DC in contact have the same or opposite signs of phase change or, say, orientation, as shown schematically in figures 3(*a*)–(*e*). Figures 3(*a*) and (*b*) show that two pieces (AB and CD) of DC with opposite orientations annihilate after their collision, but DC having the same signs can contact or cross each other along finite segments under the influence of thermal fluctuations, as shown in figures 3(*c*)–(*e*).

The number density per unit time of collisions between DC increases with increasing temperature. As a result, some DC loops can be observed, as shown in the lower left-hand side of figure 2(*b*). This process may be the reason for the weak dip of the δ curve versus temperature below 230 °C given in [6]. As a consequence, the collision of DC reduces the configurational entropy via a reduction of the density of DC, and therefore the value of δ proportional to the density of DC will decrease with increasing temperature. Because the wall-wandering fluctuations have insignificant effects for small δ in three-dimensional systems [16, 17] and because the density of DC with negative phase jumps, resulting from the rare occurrence of re-entrant DC configuration as shown in figure 5 in [18], is low, δ exhibits only a slight fall during heating below 230 °C. When reaching a temperature just above T_L, nuclei of DC were observed (figure 2(*c*)), which were studied in detail in a previous paper [11].

The evolution of newly created DC in BSN during the heating run is demonstrated in figures 4(*a*)–(*f*). Figure 4(*a*) is taken at ambient temperature and shows the configuration of frozen-in DC which are randomly distributed in the crystal due to strong pinning on defects in BSN. Figure 4(*b*) shows the appearance of DC nuclei at about 230 °C, and figure 4(*c*), taken at the same temperature, after several minutes, as figure 4(*b*), shows the growth of DC nuclei leading to thermal equilibrium configuration. Figures 4(*d*) and (*e*) were taken at about 250 °C, separated by a time interval of several minutes, and figure 4(*f*) at about 260 °C.

The dynamic pattern evolution of DC was recently studied by Kawasaki *et al* [18] by means of computer simulation of model dynamic equations. The results reported for a special case of single q modulation agree in many respects with the ones reported above in BSN (figures 4(*a*)–(*f*)). However, the nucleus (termed stripple in [18], and in the following used for the extended nucleus of DC, a pair of vortices connected by four DC as shown in figure 5) in BSN consists of four DC instead of three DC there. It was reported previously [11] that the nucleus in BSN grows easily by horizontal extension, i.e. perpendicular to the modulation wavevector. This corresponds to the case without interactions between the vortex and the DC in [18]. As the droplet-like nuclei of DC (figure 4(*b*)) extend horizontally, they coalesce with each other (figure 4(*c*)) by head-on collision or general encounter of two stripples (refer to figures 7 and 8 in [18]). From figure 4 one finds the following phenomenon. The frozen-in DC are randomly distributed in the crystal and start meandering near T_L by thermal fluctuations. However, the newly created stripples come into existence with an average direction perpendicular to the modulation wavevector, and thus they intersect the frozen-in DC there.

Figure 5 schematically illustrates one of the possible situations occurring around a line segment of a DC (AB in figure 4(*a*)). As a vortex of the stripple approaches the

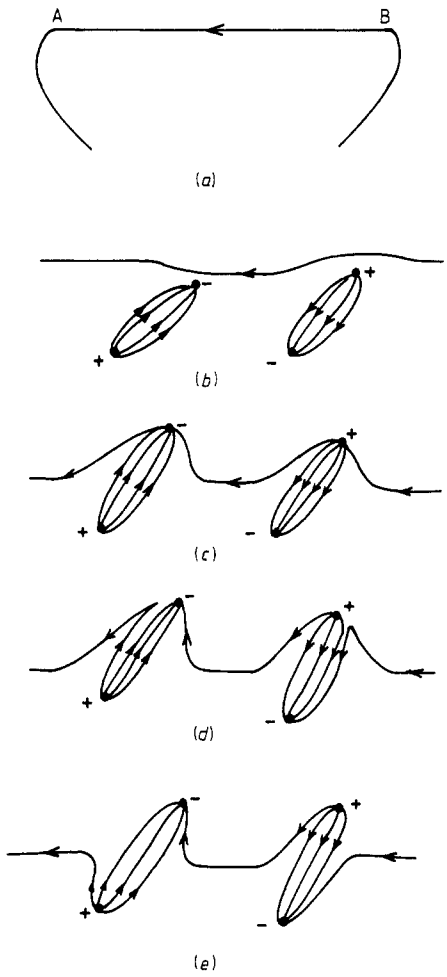

Figure 5. Schematic plot of encounter of a curved DC and a stripple of DC nucleus having the same sign (right) and opposite sign (left) of phase change.

curved DC from one side driven by the misfit force, the upper outer DC of the stripple undergoes attraction from the lower part of the curved DC, on the assumption that there exists an attractive interaction between the DC over considerable distances, but a repulsive one at short distances (see the following section). Then the vortices in figure 5(*b*) turn upwards in response to the attraction. The top DC of the stripple are still subject to a repulsive force with the curved DC, which is now deformed in a way to lower the interaction energy further at the expense of its domain-wall energy just before reconnection takes place (as shown in figures 5(*c*), (*d*) and (*e*)). After that the two vortices move away from the curved DC, and they may encounter other stripples. As a consequence of these processes, and due to meandering and collisions of DC under the influence of thermal fluctuations, no regular DC lattice exists in BSN. Thus, the wavy DC arrays shown in figure 4(*e*) were the only type observed. When the vortex of a stripple approaches a ferroelastic domain wall in BSN, the situation shown in figure 6 similar to that described in figure 13 in [18] may occur, as was already indicated [11]. After crossing the domain wall the stripple reorients into the direction perpendicular to the previous one.

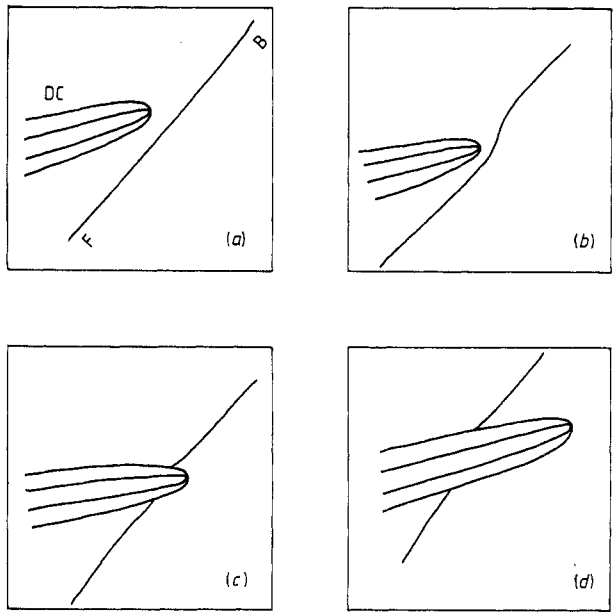

Figure 6. Crossing process of a stripple through a ferroelastic domain boundary (FB) taking place in the successive steps (*a*), (*b*), (*c*) and (*d*). The final stage of reorientation of the stripple is not indicated.

According to the experimental observations presented, the following picture of the C–I transition is suggested. As the transition from the C phase is initiated, nuclei made up by four DC are successively nucleated in the homogeneous C phase and the crystal is gradually filled up with clusters of DC. It takes a very long time for the system to reach the final equilibrium state during the relaxation process. As the number of DC in the crystal increases and the equilibrium state is approached, a rough and wavy DC array is formed, with an average direction of the DC lines perpendicular to the modulation wavevector. In the following a thermodynamic interpretation of these features is presented based on a phenomenological Landau approach.

4. Qualitative theory of C–I transition

Following the experimental results available, the I phase in BSN exhibits a wavy DC array, which may be considered as a multi-soliton lattice near T_L, and the processes during C–I transition involve nucleation or annihilation of DC. Thus the phase-modulation-only (PMO) approximation of Landau theory is likely to account for the experimental results.

The explicit form of BSN free-energy expansion as well as its qualitative consequences on its static properties have already been given by Toledano *et al* [19] and Schneck *et al* [6]. In order to explain the elastic properties of incommensurate BSN, three types of corrections were considered by Errandonea *et al* [20]: a coupling between the strains and the fluctuations of the modulus of the order parameter (OP), a dispersive coupling between the strains and the amplitude mode, and the influence of defects. In this section, we shall mainly discuss the interaction between the DC and the phenomena occurring

during the lock-in (or C–I) transition within the framework of the Landau theory and within the PMO approximation.

For a given modulation vector $\boldsymbol{k}$, the symmetry properties of the OP are described by an irreducible representation $\Gamma_{m(\boldsymbol{k}^*)}$ of the high-symmetry space group G_0, where $\boldsymbol{k}^*$ is a star of vectors of the first Brillouin zone containing the modulation vector $\boldsymbol{k}$. The index m specifies a small representation of the little group $G_{\boldsymbol{k}}$ associated with $\boldsymbol{k}$. According to Toledano *et al* [6], the star in BSN contains four non-equivalent vectors $\pm\boldsymbol{k}_i$ and $\pm\boldsymbol{k}_i'$, where

$$\begin{aligned}\boldsymbol{k}_i &= \tfrac{1}{4}(1+\delta)(\boldsymbol{a}^*+\boldsymbol{b}^*)+\boldsymbol{c}^*/2\\ \boldsymbol{k}_i' &= \tfrac{1}{4}(1+\delta)(\boldsymbol{a}^*-\boldsymbol{b}^*)+\boldsymbol{c}^*/2\end{aligned} \tag{1}$$

which are incommensurable with the reciprocal-lattice periods of the symmetrical phase. For the components of the OP we take the normal coordinates $Q_{1(\boldsymbol{k})}$, $Q_{1(\boldsymbol{k})}^*$, $Q_{2(\boldsymbol{k}')}$, $Q_{2(\boldsymbol{k}')}^*$. Here we have already simplified the problem from originally four complex amplitude fields to two by taking complex-conjugate amplitudes for $+\boldsymbol{k}_i$ and $-\boldsymbol{k}_i$, and similarly for $+\boldsymbol{k}_i'$ and $-\boldsymbol{k}_i'$. Using the notation $Q_1=\rho e^{i\varphi}$, $Q_2=\rho' e^{i\varphi'}$, where (ρ,φ) and (ρ',φ') are coordinate-dependent, the average free-energy density f is given by [6]

$$f=\int (f_0'+f_1'+f_1'')\,\mathrm{d}^3r \Big/ \int \mathrm{d}^3r \tag{2}$$

where

$$\begin{aligned}f_0 = {}& \tfrac{1}{2}\alpha(\rho^2+\rho'^2)+\tfrac{1}{4}\beta_1(\rho^4+\rho'^4)+\tfrac{1}{4}\beta_2[\rho^4\cos(4\varphi)+\rho'^4\cos(4\varphi')]\\ &+\tfrac{1}{2}\beta_3\rho^2\rho'^2+\lambda\left(\rho^2\frac{\partial\varphi}{\partial x}+\rho'^2\frac{\partial\varphi'}{\partial y}\right)\\ &+K_1\left[\rho^2\left(\frac{\partial\varphi}{\partial x}\right)^2+\left(\frac{\partial\rho}{\partial x}\right)^2+\rho'^2\left(\frac{\partial\varphi'}{\partial y}\right)^2+\left(\frac{\partial\rho'}{\partial y}\right)^2\right]\\ &+K_2\left[\rho^2\left(\frac{\partial\varphi}{\partial y}\right)^2+\left(\frac{\partial\rho}{\partial y}\right)^2+\rho'^2\left(\frac{\partial\varphi'}{\partial x}\right)^2+\left(\frac{\partial\rho'}{\partial x}\right)^2\right]\end{aligned} \tag{3}$$

$$\begin{aligned}f_1' = {}& \tfrac{1}{2}C_{11}(e_1^2+e_2^2)+C_{12}e_1e_2+C_{13}(e_1+e_2)e_3+\tfrac{1}{2}C_{33}e_3^2+\tfrac{1}{2}C_{44}(e_4^2+e_5^2)\\ &+\tfrac{1}{2}C_{66}e_6^2+\lambda_1'\mathrm{O}(e_ie_je_k)+\lambda_2'\mathrm{O}(e_i^2e_j^2)\end{aligned} \tag{4}$$

$$f_1''=[\mu_1(e_1+e_2)+\mu_3e_3](\rho^2+\rho'^2)+\nu(e_1-e_2)(\rho^2-\rho'^2). \tag{5}$$

This representation applies to the reference frame whose orientation is adjusted to the principal crystallographic axes of the orthorhombic phase, i.e. x, y and z coordinates correspond to the orthorhombic axes a_0, b_0 and c_0. Here f_0' is the usual free-energy expansion applying to the bare OP, i.e. uncoupled to strains. The first four terms in (3) correspond to the homogeneous OP expansion, the fifth term with the λ coefficient is the 'Lifschitz invariant', which favours the onset of the I phase, and the last two terms favour the onset of the C phase. In (4) f_1' is the elastic energy, where e_1, e_2, e_3, e_4, e_5 and e_6 correspond to the components of the deformation tensor u_{11}, u_{22}, u_{33}, u_{23}, u_{13} and u_{12}, respectively, which are expressed in terms of the elastic displacement vector $\boldsymbol{u}$ according

to the relation

$$u_{ij} = \frac{1}{2}\left(\frac{\partial u_i}{\partial x_j} + \frac{\partial u_j}{\partial x_i}\right).$$

The coefficients $C_{11}, C_{22}, \ldots$ represent Hooke's tensor in the notation of Voigt. The last terms of f_1' represent anharmonic interactions. In (5) f_1'' contains the lowest-order coupling terms between the strains and the OP amplitudes. Up to now the coupling terms between the OP phases and the strains have not been considered in the free energy of the I phase. Indeed, when a Lifschitz invariant [21] exists, it will necessarily give rise to coupling terms with totally symmetric strain components. In BSN the contribution of these coupling to the free energy will be of the form

$$f_2' = [\tfrac{1}{2}(\gamma_1 + \gamma_2)(e_1 + e_2) + \gamma_3 e_3]\left(\rho^2 \frac{\partial \varphi}{\partial x} + \rho'^2 \frac{\partial \varphi'}{\partial y}\right)$$
$$+ \tfrac{1}{2}(\gamma_1 - \gamma_2)(e_1 - e_2)\left[\rho^2\left(\frac{\partial \varphi}{\partial x} + \frac{\partial \varphi}{\partial y}\right) - \rho'^2\left(\frac{\partial \varphi'}{\partial y} - \frac{\partial \varphi'}{\partial x}\right)\right]. \tag{6}$$

We now consider first the phase diagram of the incommensurate BSN in the approximation where no harmonics of the basic periodicity are taken into account. The free energy of the I phase becomes

$$f_I = \tfrac{1}{2}\alpha(\rho^2 + \rho'^2) + \tfrac{1}{4}\beta_1(\rho^4 + \rho'^4) + \tfrac{1}{2}\beta_3\rho^2\rho'^2 \tag{3a}$$

and does not depend on the phase variables φ and φ'. Thus, two possible phases are obtained by minimising the free energy (3*a*) for $\alpha < 0$ (i.e. for $T < T_I$): (i) $\rho^2 = (-\alpha/\beta_1), \rho'^2 = 0$ or $\rho^2 = 0, \rho'^2 = (-\alpha/\beta_1)$; (ii) $\rho^2 = \rho'^2 = -\alpha/(\beta_1 + \beta_3)$. The two phases are incommensurate. Phase I corresponds to non-zero values for OP components associated with a single pair of opposite wavevectors, respectively $(\pm \boldsymbol{k})$ or $(\pm \boldsymbol{k}')$. The term $\nu(e_1 - e_2)(\rho^2 - \rho'^2)$ in (5) shows that in phase I the spontaneous strain $(e_1 - e_2)$ is non-zero, and that it has opposite values in the two possible states. Phase I is an I phase modulated in a single direction and it involves ferroelastic domains differing in the direction of the modulation as well as in the value of the spontaneous strain. Phase II corresponds to the freezing-in of all the vectors of the star of wavevectors $\boldsymbol{k}^*$. It is incommensurately modulated along both x and y directions. There exists no spontaneous strain and the average symmetry is that of the N phase.

This phase diagram is consistent with the recent studies of the coexistence of two I phases in BSN between T_L and T_I [22, 23]. One of them (1q phase) is modulated along a single direction a_0 (i.e. x), with a well oriented DC pattern above T_L. The modulations in the two kinds of ferroelastic domains are perpendicular to each other, and lock into a C phase at T_L. The increase of the incommensurability around T_L can be related to the increase of the density of DC [8]. The other one (2q phase) is modulated along both a_0 and b_0 (i.e. x and y) directions, and develops from the 1q phase above T_L on heating. At T_I the 2q phase (i.e. phase II) is stable, because its average symmetry is that of the N phase. On cooling, 1q phase (i.e. phase I) appears and the 2q phase becomes metastable, due to the increase of the spontaneous strain, which stabilises the 1q phase and suppresses the 2q phase. Therefore, near T_L only the 1q phase is observed. In the following, we study the basic physical phenomena of the I phase in BSN near the C–I transition, where, as mentioned above, only phase I is stable. Thus, we assume that $\rho \neq 0$, $\rho' = 0$ (or equivalently $\rho' \neq 0, \rho = 0$).

Neglecting the coupling between the OP moduli and the strains, the free-energy density below T_I assumes in BSN a form within the PMO approximation of the type

$$f = \int (f_0 + f_1 + f_2)\, \mathrm{d}^3 r \Big/ \int \mathrm{d}^3 r. \tag{7}$$

Here f_0 is obtained from f_0' by taking $\rho \neq 0$, $\rho' = 0$; f_1 is the same as f_1' modulo the cross term $C_{13}(e_1 + e_2)e_3$, which will only complicate the calculation but not affect the main results; and f_2 has the form

$$f_2 = (\gamma_1 e_1 + \gamma_2 e_2 + \gamma_3 e_3)\rho^2 \frac{\partial \varphi}{\partial x} + \tfrac{1}{2}(\gamma_1 - \gamma_2)(e_1 - e_2)\rho^2 \frac{\partial \varphi}{\partial y}. \tag{6a}$$

We ignore for the time being the y dependence of the phase $\varphi(x, y)$. This is based on the assumption that $K_2 \gg K_1$ holds in (3), and implies that the nucleation phenomena related to stripples cannot be described within such an approximation, because no vortices can be described without φ having y dependence. The assumption $K_2 \gg K_1$, however, favours a DC orientation perpendicular to the modulation wavevector $\boldsymbol{k}$ and suppresses curved DC. After minimising f_0 with respect to the variable $\varphi(x)$ we obtain the following sine–Gordon equation:

$$\frac{\upsilon\ \varphi}{\partial x^2} = -\frac{\beta_2}{2K_1}\rho^2 \sin(4\varphi) \tag{8}$$

which is known to have solitary solutions $\varphi_0(x)$ [24].

By means of the soliton formalism, the free-energy density f_0 can be approximated [24] in the form

$$\int f_0\, \mathrm{d}^3 r \Big/ \int \mathrm{d}^3 r - f_C = -\sigma A(T - T_C)n_0 + 4\sigma n_0\, \mathrm{e}^{-w/n_0} \tag{9}$$

where f_C is the free-energy density of the C phase, $f_C = f_0(T_C)$, n_0 and $1/w$ are, respectively, the number of solitons (DC) per unit length and the width of the soliton, and A and σ are suitable constants. The coefficient of n_0 in the first term of (9) determines the bare free energy per soliton. This free energy is positive in the C phase, vanishes at the transition temperature T_C and is negative in the I phase and thus describes the formation of solitons in the I phase. T_C corresponds roughly to T_L in table 1, but will be modified by strain and solitons (see (17) below). The second term in (9) determines the repulsive interaction energy of solitons. This term is positive and is a consequence of 'excluded-volume' effects of solitons. Thus, the solution obtained in the PMO approximation describes a continuous transition from the I to the C phase. Note that $4 \geqslant A(T - T_C)$ is required in (9) in order that the free energy is bounded from below for $n_0 \to \infty$. In case this inequality cannot be satisfied, (9) must be supplemented by additional positive terms of order $n^{1+\varepsilon}$, $\varepsilon > 0$, in order to stabilise the system. The precise value of n_0 is determined from the requirement

$$\left.\frac{\partial f}{\partial n}\right|_{n_0} = 0 = -\sigma A(T - T_C) + 4\sigma\, \mathrm{e}^{-w/n_0}\left(1 + \frac{w}{n_0}\right) \tag{9a}$$

which under the restrictive condition given above ensures $\partial^2 f/\partial n^2|_{n_0} > 0$ and therefore thermodynamic stability.

We briefly make a few remarks with respect to the two-dimensional sine–Gordon

equation obtained from

$$f_0^{(2)} = \frac{\beta_2}{4}\rho^4 \cos(4\varphi) + \lambda\rho^2 \frac{\partial\varphi}{\partial x} + K_1\rho^2 \left(\frac{\partial\varphi}{\partial x}\right)^2 + K_2\rho^2 \left(\frac{\partial\varphi}{\partial y}\right)^2,$$

and being of the form

$$\frac{\partial^2\varphi}{\partial x'^2} + \frac{\partial^2\varphi}{\partial y'^2} + \sin(4\varphi) = 0 \tag{8a}$$

where we used the rescaled variables

$$x' \equiv \frac{x}{2}\left(\frac{\beta_2}{K_1}\rho^2\right)^{1/2} \qquad y' \equiv \frac{y}{2}\left(\frac{\beta_2}{K_2}\rho^2\right)^{1/2}.$$

Equation (8*a*) has the two simple types of soliton solutions $\varphi_1 = \varphi(x)$ and $\varphi_2 = \varphi(y)$ governed by (8) and a similar equation with x replaced by y, respectively. Solutions of (8*a*) with a dependence on x and y are responsible for the stripples and vortex structure observed. This can be seen as follows. A vortex solution of (8*a*) with the third term ignored is

$$\psi(x, y) = \sum_i \sigma_i \tan^{-1}\left(\frac{y - y_i}{x - x_i}\right) \qquad \sigma_i = \pm 1, \pm 2, \ldots.$$

The σ_i represent the vortex strengths. Observe now that $\psi(x, y)$ is also a solution of (8*a*) in the neighbourhood of $\psi(x, y) = n\pi/4$, $n = 0, 1, 2, 3, 4, 5, 6$ and 7. However, $f_0^{(2)}$ will favour phase angles ψ, corresponding to $n = 1, 3, 5$ and 7. Accordingly the map d: $\psi \rightarrow \varphi$ which deforms $\psi(x, y)$ into $\varphi(x, y)$ will impose onto ψ an additional soliton structure at lines originating from the vortices, where n changes by ± 2. These lines correspond to the solitons of (8) and represent the four-fold stripples in figure 3. The fact that the stripples grow perpendicular to the wavevector $\boldsymbol{k}$ (see e.g. figure 3) is a consequence of the rescaling from x' and y' to x and y, respectively, with $K_2 \gg K_1$. A uniform stripple in the coordinates of (8*a*) is stretched along the y direction, which is perpendicular to $\boldsymbol{k}$. For a qualitative treatment of (8*a*) see Holz [25]. Let us point out that a coupling to strain will lead to an additional deformation of $\varphi(x, y)$ but will not change its topological structure.

Now we come back to our main topic and take the influence of the coupling between the phase of modulation and the strains into account. From (7) we obtain the set of Euler–Lagrange equations:

$$2K_1\rho^2 \frac{\partial^2\varphi}{\partial x^2} + 2K_2\rho^2 \frac{\partial^2\varphi}{\partial y^2} + \beta_2\rho^4 \sin(4\varphi) + \gamma_1\rho^2 \frac{\partial^2 u_x}{\partial x^2} + \gamma_2\rho^2 \frac{\partial^2 u_y}{\partial x\,\partial y} + \gamma_3\rho^2 \frac{\partial^2 u_z}{\partial x\,\partial y}$$
$$+ \tfrac{1}{2}(\gamma_1 - \gamma_2)\rho^2 \left(\frac{\partial^2 u_x}{\partial x\,\partial y} - \frac{\partial^2 u_y}{\partial y^2}\right) = 0 \tag{10a}$$

$$C_{11}\frac{\partial^2 u_x}{\partial x^2} + C_{12}\frac{\partial^2 u_y}{\partial x\,\partial y} + \tfrac{1}{4}C_{66}\left(\frac{\partial^2 u_x}{\partial y^2} + \frac{\partial^2 u_y}{\partial x\,\partial y}\right) + \tfrac{1}{4}C_{44}\left(\frac{\partial^2 u_x}{\partial z^2} + \frac{\partial^2 u_z}{\partial x\,\partial z}\right)$$
$$= -\tfrac{1}{2}(\gamma_1 - \gamma_2)\rho^2 \frac{\partial^2\varphi}{\partial x\,\partial y} - \gamma_1\rho^2 \frac{\partial^2\varphi}{\partial x^2} \tag{10b}$$

$$C_{11}\frac{\partial^2 u_y}{\partial y^2} + C_{12}\frac{\partial^2 u_x}{\partial x\,\partial y} + \tfrac{1}{4}C_{66}\left(\frac{\partial^2 u_x}{\partial x\,\partial y} + \frac{\partial^2 u_y}{\partial x^2}\right) + \tfrac{1}{4}C_{44}\left(\frac{\partial^2 u_y}{\partial z^2} + \frac{\partial^2 u_z}{\partial y\,\partial z}\right)$$

$$= \tfrac{1}{2}(\gamma_1 - \gamma_2)\rho^2 \frac{\partial^2 \varphi}{\partial y^2} - \gamma_2 \rho^2 \frac{\partial^2 \varphi}{\partial x\, \partial y} \tag{10c}$$

$$C_{33} \frac{\partial^2 u_z}{\partial z^2} + \tfrac{1}{4} C_{44} \left(\frac{\partial^2 u_x}{\partial x\, \partial z} + \frac{\partial^2 u_z}{\partial x^2} + \frac{\partial^2 u_z}{\partial y^2} + \frac{\partial^2 u_y}{\partial y\, \partial z} \right) = 0. \tag{10d}$$

For the sake of simplicity we have ignored the z dependence of the phase variable φ. Presumably, these equations cannot be solved analytically in general.

Formally the set of equations (10) may be solved by using the elastic Green function obeying suitable boundary conditions for the homogeneous part of (10*b*) to (10*d*) and expressing the solution in the form

$$u_\alpha(\boldsymbol{r}) = \int \mathrm{d}^3 r' G_{\alpha\beta}(\boldsymbol{r}, \boldsymbol{r}') f_\beta(\boldsymbol{r}').$$

Here $f_\beta(\boldsymbol{r})$ represents the right-hand side of equations (10*b*) to (10*d*) respectively with $\beta = x, y, z$. Putting $u_\alpha(\boldsymbol{r})$ into (10*a*) yields an integro-differential equation for φ. In a representation corresponding to (8*a*) one obtains

$$\frac{\partial^2 \varphi}{\partial x'^2} + \frac{\partial^2 \varphi}{\partial y'^2} + \int \mathrm{d}^3 r'' \left(g_{xx}(\boldsymbol{r}'', \boldsymbol{r}') \frac{\partial^2 \varphi}{\partial x''^2} + 2 g_{xy}(\boldsymbol{r}'', \boldsymbol{r}') \frac{\partial^2 \varphi}{\partial x''\, \partial y''} + g_{yy}(\boldsymbol{r}'', \boldsymbol{r}') \frac{\partial^2 \varphi}{\partial y''^2} \right)$$
$$+ \sin(4\varphi) = 0. \tag{8b}$$

Here the coefficient functions $g_{\alpha\beta}(\boldsymbol{r}'', \boldsymbol{r}')$ are obtained from the Green function over two partial differentiations. Because $G_{\alpha\beta}(\boldsymbol{r}, \boldsymbol{r}') \sim \ln|\boldsymbol{r} - \boldsymbol{r}'|$ for the two-dimensional problem, the third term in (8*b*) provides for a strongly non-local coupling with possible log-type divergences. The solutions of (8*b*) will be of the same topological type as $\psi(x, y)$ given earlier subject to the deformations produced by the two last terms in (8*b*). For the case $\varphi(x, y) = \varphi(x)$ a considerable simplification arises, because (8*b*) will reduce to (13).

Using now the simplifying assumption that the modulation in BSN occurs only in the x direction, i.e. $\varphi = \varphi(x)$, we look first for a solution of (10) based on the *ansatz* [3]

$$\begin{aligned} u_x &= \tilde{u}_x(x) + \eta_1 x + \eta_2 y + \eta_3 z + \eta_4 \\ u_y &= \tilde{u}_y(x) + \xi_1 x + \xi_2 y + \xi_3 z + \xi_4 \\ u_z &= \tilde{u}_z(x) + \zeta_1 x + \zeta_2 y + \zeta_3 z + \zeta_4 \end{aligned} \tag{11}$$

where the linear and constant coordinate terms are used to satisfy boundary conditions imposed on the system. Inserting (11) into (10) yields

$$\tilde{u}_x = -\frac{\gamma_1}{C_{11}} \rho^2 \varphi(x) \qquad \tilde{u}_y = \tilde{u}_z = 0 \tag{12}$$

$$\begin{aligned} \frac{\partial^2 \varphi}{\partial x^2} &= -\frac{\beta_2}{2K_1'} \rho^2 \sin(4\varphi) \\ K_1' &= K_1 - \frac{\gamma_1^2}{2C_{11}}. \end{aligned} \tag{13}$$

Since (13) has the same form as (8) we again obtain the wall-type picture for φ and hence also for u_x.

In order to determine the constants $\eta_1, \ldots, \zeta_4$ from the boundary conditions we first

exclude global translations and rotations of the system, implying

$$\eta_4 = \xi_4 = \zeta_4 = 0 \qquad \int (\nabla \times \boldsymbol{u})\, \mathrm{d}^3 r = 0.$$

The remaining constants follow from the equilibrium condition between the internal and external stress σ^e imposed on the system

$$\sigma^e_{\alpha\beta} = \int \frac{\partial f}{\partial u_{\alpha\beta}} \mathrm{d}^3 r \Big/ \int \mathrm{d}^3 r. \tag{14}$$

From (14) we obtain using the notation

$$\int \frac{\partial \varphi}{\partial x} \mathrm{d}^3 r \Big/ \int \mathrm{d}^3 r \equiv \frac{2\pi}{p} \Delta n$$

($p = 4$ in BSN), where $\Delta n \equiv n_+ - n_-$ represents the density difference between positive and negative DC,

$$\begin{aligned}
\eta_1 &= \frac{C_{12}}{C_{11}^2 - C_{12}^2}\left(\frac{C_{11}}{C_{12}}\sigma^e_{xx} - \sigma^e_{yy} + \frac{C_{11}\gamma_2 - C_{12}\gamma_1}{C_{11}}\rho^2 \Delta n \frac{\pi}{2}\right) \\
\xi_2 &= \frac{-C_{11}}{C_{11}^2 - C_{12}^2}\left(\frac{C_{12}}{C_{11}}\sigma^e_{xx} - \sigma^e_{yy} + \frac{C_{11}\gamma_2 - C_{12}\gamma_1}{C_{11}}\rho^2 \Delta n \frac{\pi}{2}\right) \\
\zeta_3 &= \frac{1}{C_{33}}\left(\sigma^e_{zz} - \gamma_3 \rho^2 \Delta n \frac{\pi}{2}\right) \\
\xi_3 &= \zeta_2 = 2\sigma^e_{yz}/C_{44} \\
\eta_3 &= \zeta_1 = 2\sigma^e_{xz}/C_{44} \\
\eta_2 &= \xi_1 = 2\sigma^e_{xy}/C_{66}.
\end{aligned} \tag{15}$$

This implies that the homogeneous deformations (e_1, e_2, e_3) depend on the density difference Δn of solitons, but not on their space distribution in the system. Substituting u_x, u_y, u_z into (4) modulo the cross term $C_{13}(e_1 + e_2)e_3$ and (6*a*) and adding the free energy corresponding to (13) we obtain for the free-energy change in the case of zero external stress

$$\begin{aligned}
\Delta f_I = f_I - f_C = &-\sigma' A'(T - T'_C)n + 4\sigma' n\, \mathrm{e}^{-w'/n} \\
&- D(\Delta n)^2 + \lambda'_1(\Delta n)^3 + \lambda'_2(\Delta n)^4
\end{aligned} \tag{16}$$

where $n \equiv n_+ + n_-$ and

$$D \equiv \frac{1}{2}\left(\frac{(C_{11}\gamma_2 - C_{12}\gamma_1)^2}{C_{11}(C_{11}^2 - C_{12}^2)} + \frac{\gamma_3^2}{C_{33}}\right)\left(\rho^2 \frac{\pi}{2}\right)^2.$$

The first additional term $-D(\Delta n)^2$ in (16) describes an attractive interaction between the DC mediated by the strain, whereas the term $\lambda'_1(\Delta n)^3$ breaks the symmetry with respect to $\Delta n \gtrless 0$. The term $\lambda'_2(\Delta n)^4$ stabilises the system with $\lambda'_2 > 0$. Equation (16) indicates that DC of the same sign are mutually attracted and consequently the distance between DC remains finite at the transition point, which may lead to a discontinuity of the C–I transition, in agreement with the experimental results observed in BSN. Note that the primed coefficients σ', A', T'_C and w' are supposed to be computed from the statistical

mechanics of the sine–Gordon model with coupling constants given by (13), supplemented by inhomogeneous strain terms, similarly to the way in which (9) is computed from (8), and $n_\pm$ is computed from an equation analogous to (9*a*), where $4 \geqslant A'(T - T'_C)$ has also to be satisfied. Extremal solutions to (16) are obtained from $\partial \Delta f_I / \partial n_+ = \partial \Delta f_I / \partial n_- = 0$. For the sake of simplicity we will take $n \simeq \Delta n$.

From the condition that the free energy in the I phase equals that in the C phase, and setting $n \simeq \Delta n$, we obtain

$$-\sigma' A'(T_L - T'_C)n + 4\sigma' n\, e^{-w'/n} - Dn^2 + \lambda'_1 n^3 + \lambda'_2 n^4 = 0.$$

Near the transition temperature, we have $w'/n \gg 1$ and $n \ll 1$; thus we obtain the C–I transition temperature T_L

$$T_L \simeq T'_C - \frac{Dn_L}{\sigma' A'} < T'_C \tag{17}$$

where n_L is the soliton density at T_L. Now the characteristics of the C–I transition may be shown by plotting $f_I - f_C$ versus n, at different temperatures, $t \equiv (T - T_L)/(T'_C - T_L)$, as presented in figure 7. On decreasing the temperature from the I phase, the system

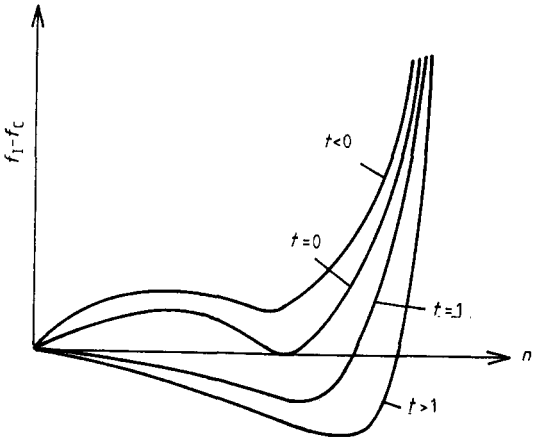

Figure 7. Schematic plot of free-energy difference $f_I - f_C$ from (16) as a function of the DC (or soliton) density n, at different temperatures. The parameter t is the reduced temperature.

enters the C phase at T_L, with a discontinuous change of n. Conversely, on increasing the temperature from the C phase, although the free energy favours the I phase, the nucleation of DC requires a certain thermal activation due to the positive energy of DC at $T < T'_C$. This leads to a thermal hysteresis. In consideration of the influence of thermal fluctuations, there should be coexistence of both C and I phases at $T_L < T < T'_C$.

We would like to point out that Bjelis and Barisic have developed a non-linear model for the hysteresis in tetrathiafulvalene tetracyanoquinodimethane (TTF-TCNQ) based on equations for phase and amplitude solitons [26]. Translated into our model, such an analysis would require, instead of $Q_1(\boldsymbol{k})$ and $Q_2(\boldsymbol{k})$, as explained below (1), use of two fields $Q_{1,\pm} = \rho_\pm e^{i\varphi_\pm}$ corresponding to two phase variables $\beta \sim \varphi_+ - \varphi_-$ and $\theta \sim \tan^{-1}(\rho_+/\rho_-)$. Although such a theory may also apply to the present system we have not worked it out so far.

In general, hysteretic phenomena are connected with first-order phase transitions and the latter with nucleation phenomena. It seems reasonable to assume that the nucleation of stripples drives the discontinuous phase transition at T_L and that such

processes are also responsible for the hysteretic effects and chaotic state of DC patterns. The one-dimensional analysis presented in this work may be considered as a type of mean-field approximation mainly dictated by the wish to reduce the complexity of the theory.

For the one-dimensional problem Barisic and Batistic have developed a theory of a first-order C–I transition in the presence of charged solitons interacting via $1/r$ Coulomb forces [27]. In the present theory DC are not charged but the strain provides for a long-range interaction. In the one-dimensional sine–Gordon equation (13) this is not the case, because coupling to strain yields a change of the coupling constant such that the width of solitons is decreased. The attractive thermodynamic interaction between solitons mediated by strain and described by the third term in (16) is a consequence of long-range interaction and the boundary conditions imposed on the strain field, as can be seen from (10*b*) in the form

$$\partial^2 u_x/\partial x^2 = -(\gamma_1 \rho^2/C_{11})\,\partial^2 \varphi/\partial x^2. \tag{10e}$$

Because the general solution of this differential equation for given $\varphi(x)$ is the sum of a particular integral and the general homogeneous solution $u_x^h = \eta_1 x + \eta_4$, the boundary conditions play an important role in fixing u_x^h. The solitons act as sources of the Coulomb-like strain field. Bound states of solitons as in breathers are a consequence of short-range interaction. Long-range interaction as considered in [27] appears also in (8*a*) and is of a logarithmic type (see e.g. Holz [25]). Similar arguments apply to (8*b*), where the integral operator will yield an additional attractive interaction between solitons.

Concerning the attractive interaction of DC the following additional remarks will be made. Although the left-hand sides of (10*e*) and (8) involve one-dimensional Laplace operators, the effect in both equations is different. Owing to the right-hand side in (8) solitons are topologically stabilised and attract or repel each other over short range when they have the opposite or same sign, respectively. Furthermore, independent of the boundary conditions on the φ variable, there can be no solution of the linear type $\varphi = (2\pi/p)\Delta n x + \varphi_0$ leading to a $(\Delta n)^2$ term in the free energy. In (10*e*) this is not the case and one obtains a long-range Coulomb-like interaction between sources and sinks whose force is independent of distance. This force will be attractive for solitons of the same sign and repulsive for solitons of opposite sign. Because a wavy DC array consists essentially of solitons of the same sign, the situation is similar to that in gravitationally bounded systems, where the hard core repulsion (or centrifugal force) keeps the system from collapsing. A qualitatively different situation applies to the two- or quasi-two-dimensional problem, because there already the soliton equation (8*a*) provides for long-range interaction between vortices (vortex loops) and is of the $\ln(1/r)$ type, whereas interactions among DC will depend on their shape and are of short range. However, when strain is taken into account, DC will interact over long range.

We recall that we have neglected the coupling between the strains and the moduli of the OP given by f_1'' in (5), in the calculations presented above, which however does not affect the qualitative results. This coupling will give an additional contribution to the spontaneous value for $(e_1 - e_2)$ representing the breaking of the macroscopic symmetry

$$\Delta e = \int (e_1 - e_2)\,\mathrm{d}^3 r \Big/ \int \mathrm{d}^3 r = \frac{-\rho^2}{C_{11} - C_{12}} \left(\nu + \frac{\pi}{2}(\gamma_2 - \gamma_1)\Delta n \right). \tag{18}$$

From (18) it follows that the spontaneous value for $(e_1 - e_2)$ is proportional to the DC density Δn; hence it develops a discontinuity during the lock-in transition, and a large thermal hysteresis similar to that derived for n, in agreement with the experimental

results on the measurement of birefringence $(n_a - n_b)$ [28]. One also shows that the application of external pressure does not remove the discontinuity at the lock-in transition, but only changes the value of T_C'. For a sufficiently large anisotropic stress $(\sigma_{xx}^e - \sigma_{yy}^e)$, the I phase can be suppressed completely, which is consistent with the experimental measurement of birefringence $(n_a - n_b)$ under the application of a uniaxial stress (along b_0) in BSN (figure 3 in [29]).

It has been noted that in incommensurate insulators defects stabilise the incommensurate structure, destroy the long-range order in the I phase, enhance the chaotic state near the lock-in transition and increase the thermal hysteresis [30]. The main structural defect considered in BSN is represented by vacancies at the sodium sites [28]. The interaction between the defects and the incommensurate modulation results in the following remarkable features: a large thermal hysteresis affecting all physical properties occurred each time the temperature trend was reversed at any temperature within the I phase [6]; the striking memory effects [28]; and the existence of an incomplete lock-in phase below T_L.

We would like to point out that Lederer *et al* [31] have developed a theory of memory effects that is characteristic for I modulation systems and invokes the formation of a so-called defect density wave. The defect density wave is formed under 'slow experimental conditions' allowing the defects to diffuse and decorate the modulated structure at the temperature of measurement. Memory effects of all kinds are then a consequence of an impurity locked in the C phase. Effects of this kind may also play a role in the present observations because of the existence of a large number of mobile point defects (such as sodium vacancies [28]) and of defects generated by electron irradiation during observations, which may diffuse and pin the DC. It is worthwhile to point out that recent studies [22, 23] show that the large thermal hysteresis, complex memory effects and the slow relaxation in BSN are related both to the coexistence of the 1q and 2q phases and to the interaction between modulation and mobile defects. Accurately, the slow relaxation of the linewidth and intensity of satellite reflections and of the birefringence [12] are attributed to the gradual change of the system between the 1q and 2q phases. Such processes take place very slowly (typically in two or four days [12]) due to the diffusion of mobile point defects which pin the modulation wave. During a thermal cycle a large hysteresis of physical properties occurs because of incomplete relaxation. A similar mechanism accounts for the memory effect.

The strong pinning of DC by defects in BSN leads to the occurrence of a spatially chaotic state near T_L (figure 4) consisting of an inhomogeneous distribution of DC in the crystal, having stochastic shape.

A characteristic feature of DC in the I phase is that they do not form a regular soliton lattice but a wavy DC array. In the one-dimensional model discussed we have ignored this property. Obviously the defects in a regular vortex lattice are the vortices that nucleate in the form of stripples, and once the stripples become unbounded the regular DC array will be destroyed. The situation is quite similar to the melting of a crystal, which is driven by the nucleation of pairs of dislocations in two dimensions. We conjecture that the wavy DC array is a type of vortex plasma, which however does not destroy the overall orientation of the soliton lattice but only its long-range positional correlation. The situation is then similar to liquid-crystalline systems, which have a finite orientational order parameter. A theoretical analysis of the wavy DC array may be based on (8*a*), f_0 and the ratio K_1/K_2. The disappearance of the wavy DC array and its replacement by an isotropic phase also requires an analysis of the amplitudes ρ and ρ' and the mutual interaction between the vectors in (1).

5. Conclusions

In conclusion we have reported an experimental study of the dynamic evolution of DC during the C–I transition in BSN, and presented a qualitative discussion of it on the basis of the phenomenological Landau theory. It has been found that the interaction of DC of the same sign at large distances is attractive ($-D(\Delta n)^2$), but is repulsive independent of their sign at short distances ($4\sigma'\Delta n\, e^{-w'/\Delta n}$), and that frozen-in DC become meandering and collide with their neighbours to reduce the DC density at a temperature even below the lock-in transition under the influence of thermal fluctuations. A transient metastable state (or chaotic state) with an inhomogeneous distribution and stochastic conformation of DC was observed with successive nucleation of DC in the early stages of transition, forming a wavy DC array. The wavy DC array is a consequence of the network structure formed from a set of vortices interconnected by DC with a preferential direction perpendicular to modulation. DC loops with high density of DC are formed at high temperature. In the light of a phenomenological Landau theory, the coupling between the strains and the phase of OP plays an important role in incommensurate BSN. It results in an attractive interaction between DC and a discontinuity in the physical quantities (n, $e_1 - e_2$, $n_a - n_b$, etc) during the C–I transition, which is qualitatively in agreement with the experimental results available.

Acknowledgments

One of the authors (PX) would like to thank Professor H-G Unruh, Professor V Dvorak and Dr S Müller for many useful discussions. Some useful remarks by Professor A Holz on the theoretical aspects of the problem and a careful reading of the manuscript are particularly acknowledged. Partial financial support by the Deutsche Forschungsgemeinschaft within SFB130 is acknowledged.

References

[1] McMillan W L 1976 *Phys. Rev.* B **14** 1496
[2] Bruce A D, Cowley R A and Murray A F 1978 *J. Phys. C: Solid State Phys.* **11** 3591
[3] Sannikov D G 1986 *Incommensurate Phases in Dielectrics (Modern Problems in Condensed Matter Sciences 14-1)* (Amsterdam: North-Holland) p 43 and references therein
[4] Singh S, Draegert D A and Geusic J E 1970 *Phys. Rev.* B **2** 2709
[5] Giess E A, Scott B A, Burns G, O'Kane D F and Segmüller A 1969 *J. Am. Ceram. Soc.* **52** 276
[6] Schneck J, Toledano J C, Joffrin C, Aubree J, Joukoff B and Gabelotaud A 1982 *Phys. Rev.* B **25** 1766
[7] Schneck J, Primot J, Ravez J and Von der Muhl R 1977 *Solid State Commun.* **21** 57
[8] Pan Xaioqing, Feng Duan, Yao Minghui and Hu Meisheng 1985 *Phys. Status Solidi* a **91** 57
[9] Van Tendeloo G, Amelinkx S, Manolikas C and Wen Shulin 1985 *Phys. Status Solidi* a **91** 483
[10] Manolikas C, Schneck J, Toledano J C, Kiat J M and Calvarin G 1987 *Phys. Rev.* B **35** 8884
[11] Pan Xiaoqing and Feng Duan 1988 *Phys. Status Solidi* a **106** K117
[12] Toledano J C, Schneck J and Errandonea G 1986 *Incommensurate Phases in Dielectrics (Modern Problems in Condensed Matter Sciences 14-2)* (Amsterdam: North-Holland) p 233 and references therein
[13] Baree S, Mutka H, Roucau C and Errandonea G 1987 *Phase Transitions* **9** 225
[14] Feng Duan and Pan Xiaoqing 1986 *Proc. XIth Int. Conf. Electron Microscopy (Kyoto)* p 1239
[15] Pan Xiaoqing to be published
[16] Fisher M E and Fisher D S 1982 *Phys. Rev.* B **25** 3192
[17] Nattermann T 1982 *J. Physique* **43** 631

[18] Kawasaki K and Yamanaka S 1986 *Phys. Rev.* B **34** 7986
[19] Toledano J C, Schneck J and Lamborelle C 1981 *Symmetries and Broken Symmetries* ed N Boccara (Paris: IDSET) p 217
[20] Errandonea G, Hebbache M and Bonnourrier F 1985 *Phys. Rev.* B **32** 1691
[21] Golovko V A and Levanyuk A P 1983 *Light Scattering Near Phase Transitions (Modern Problems in Condensed Matter Sciences 5)* (Amsterdam: North-Holland) p 169 and references therein
[22] Pan Xiaoqing, Unruh H-G and Feng Duan 1989 *Ferroelectrics* to be published
[23] Kiat J M, Calvarin G and Schneck J 1989 *Ferroelectrics* to be published
[24] Bak P and Emery V J 1976 *Phys. Rev. Lett.* **36** 978; Bruce A D, Cowley R A and Murray A F 1978 *J. Phys. C: Solid State Phys.* **11** 3591
[25] Holz A 1979 *Physica* **97A** 75
[26] Bjelis A and Barisic S 1982 *Phys. Rev. Lett.* **48** 684
[27] Barisic S and Batistic I 1985 *J. Physique Lett.* **46** L819
[28] Errandonea G, Toledano J C, Litzler A, Savary H, Schneck J and Aubree J 1984 *J. Physique Lett.* **45** L329
[29] Schneck J, Toledano J C, Errandonea G, Lityler A, Savary H, Manolikas C, Kiat J M and Calvarin G 1987 *Phase Transitions* **9** 359
[30] Hamano K 1986 *Incommensurate Phases in Dielectrics (Modern Problems in Condensed Matter Sciences 14-1)* (Amsterdam: North-Holland) p 365 and references therein
[31] Lederer P, Montambaux G, Jamet J P and Chauvin M 1984 *J. Physique Lett.* **45** L627